AIAA JOURNAL
Vol. 43, No. 1, January 2005

Performance of Smart Damping Treatment Using Piezoelectric Fiber-Reinforced Composites

M. C. Ray*
Texas A&M University, College Station, Texas 77843-3123
and
N. Mallik†
Indian Institute of Technology, Kharagpur 721 302, India

This study deals with the active constrained layer damping (ACLD) of laminated composite plates to demonstrate the performance of piezoelectric fiber-reinforced composite (PFRC) layer as the constraining layer of ACLD treatment. A finite element model is developed for the smart composite plates integrated with the patches of ACLD treatment. The performance of the constraining PFRC layer has been investigated for active damping of thin symmetric and antisymmetric crossply and antisymmetric angle-ply laminated composite plates. The main concern of this study has been focused on investigating the significant effect of variation of piezoelectric fiber orientation in the PFRC layer on enhancing the damping characteristics of the laminated substrate plates, and the fiber angle in the PFRC layer for which the control authority of the patches becomes maximum has been determined.

I. Introduction

PIEZOELECTRIC materials have been increasingly used as distributed sensors and/or actuators for active control of vibration of high-performance lightweight smart structures during the past decade.[1–17] This increasing demand is credited to their inherent properties of direct and converse piezoelectric effects. Because of their direct piezoelectric effect, they are used as sensors because they are capable of inducing an electric potential/charge when subjected to mechanical load, and their capability of being deformed upon externally applied voltage/charge made them useful as actuators. The flexible structures when coupled with a layer/patch of these materials acting as distributed sensors and/or actuators are customarily known as "smart structures." The performance of smart structures depends on the magnitude of the piezoelectric stress/strain coefficients. The magnitudes of the piezoelectric coefficients of the existing monolithic piezoelectric materials are very low. Hence, large control voltage is necessary for achieving a significant amount of active damping in smart structures. Further research on the potential use of these existing piezoelectric materials as the distributed actuators for smart structures has led to the development of active constrained layer damping (ACLD) treatment.[18] The ACLD treatment consists of a viscoelastic constrained layer and a piezoelectric layer acting as the active constraining layer. When the treatment is integrated with a base structure (substrate) and is augmented with an appropriate control strategy, the strain of the piezoelectric constraining layer can be controlled in response to the vibration of the base structure leading to the active constrained layer damping of this structure. It is well known that the flexural vibration control by the constrained layer damping treatment is attributed to the dissipation of energy in the viscoelastic core undergoing transverse shear deformation. As the constraining layer of the activated ACLD treatment increases the passive transverse shear deformation of the viscoelastic constrained layer, the ACLD treatment improves the overall damping characteristics of the flexible structures over its passive counterpart. Because the control effort necessary to increase the shear deformation of viscoelastic layer is compatible with the low control authority of the monolithic piezoelectric materials, the piezoelectric materials perform much better to attenuate the vibration of smart structures when they are used as active constraining layer of the ACLD treatment than when they are used alone as distributed actuators. Also, ACLD treatment provides the attributes of both passive and active damping occurring in unison because of the fact that passive damping mechanism is integral to this treatment. Hence, since its inception prolific use of ACLD treatment can be noticed for efficient and reliable active control of flexible structures.[19–29]

Piezoelectric composites are now being effectively used for underwater transducers and medical imaging applications.[30–32] These composites have been reported to show improved mechanical performance, electromechanical coupling characteristics, and acoustic impedance matching with the surrounding medium over the monolithic piezoelectric materials. These composites tune the thickness mode of oscillation as their piezoelectric fibers are vertically oriented and cannot be used for flexural vibration control. The piezoelectric fiber-reinforced composites (PFRC) wherein the fibers are longitudinally oriented can serve the purpose of actuating the flexural modes of vibrations. In the recent papers,[33,34] authors investigated the effective elastic and piezoelectric properties of unidirectional PFRC materials that are useful for the analysis of plate- and beam-type smart structures, respectively. The main concern of the investigations was to predict the effective piezoelectric coefficient of the PFRC materials, which quantifies the induced normal stress in the fiber direction as a result of the applied electric field in the direction transverse to the fiber direction. It has been found that this effective piezoelectric coefficient becomes significantly larger than the corresponding coefficient of the piezoelectric material of the fibers within the useful range of fiber volume fraction. Note that this piezoelectric coefficient is mainly responsible for active control of flexural vibrations of smart structures. In a previous paper, the authors[35] carried out the static analysis of laminated composite plates integrated with a layer of this PFRC material to investigate the performance of this layer as a distributed actuator for smart structures.

In this paper, authors investigated the performance of this PFRC material for the active constrained layer damping of laminated composite plates. The novel aspect of this work is that the constraining layer of the ACLD treatment has been considered to be made of this PFRC material. A finite element model has been developed considering first-order shear deformations in all of the layers and three different equivalent single-layer theories. As a novel objective of

Received 12 January 2004; revision received 14 May 2004; accepted for publication 20 May 2004.

*Visiting Associate Professor, Department of Mechanical Engineering.
†Research Scholar, Department of Mechanical Engineering.

this study, particular emphasis has been placed on investigating the effect of fiber orientation in the PFRC layer on the active damping of thin symmetric/antisymmetric cross-ply and antisymmetric angle-ply plates using this finite element model.

II. Finite Element Model

Figure 1 shows a simply supported rectangular laminated substrate plate made of N number of orthotropic layers. The length, width, and thickness of the plate are denoted by a, b, and h, respectively. The top surface of the plate is integrated with the rectangular patches of ACLD treatment. The constraining layer of the ACLD treatment is made of PFRC material, and its constructional feature is also schematically demonstrated in Fig. 1. The thickness of the PFRC layer is h_p and that of the viscoelastic constrained layer of the ACLD treatment is h_v. The midplane of the substrate plate is considered as the reference plane. The origin of the laminate coordinate system (x, y, z) is located on the reference plane in such a way that $x = 0, a$ and $y = 0, b$ indicate the boundaries of the substrate plates. Denoting by k ($k = 1, 2, 3, \ldots, N + 2$) the layer number of any layer of the overall plate, the thickness coordinate z of the top and bottom surface of any (kth) layer are represented by h_{k+1} and h_k, respectively. The fiber orientation in any layer of the substrate plate with respect to the laminate coordinate system is denoted by θ, whereas that in the active constraining layer of the PFRC material is denoted by ψ.

First-order shear deformation theories will be used for modeling the overall plate integrated with the patches of ACLD treatment. Figure 2 describes a schematic representation of the kinematics of deformation based on these theories. As shown in this figure, u_0 and v_0 are the generalized translational displacements of a reference point (x, y) on the midplane ($z = 0$) of the substrate along x and y axes, respectively; θ_x, ϕ_x, and γ_x are the generalized rotations of the normals to the middle planes of the substrate, viscoelastic layer, and the PFRC layer, respectively, about the y axis and the generalized rotations of these normals about x axis are denoted, respectively, by θ_y, ϕ_y, and γ_y. According to the kinematics of deformation shown in Fig. 2 and using the appropriate singularity functions, the axial displacements u and v at a point in any layer of the overall plate along x and y directions, respectively, can be written as

$$u(x, y, z, t) = u_0(x, y, t) + (z - \langle z - h/2\rangle)\theta_x(x, y, t) + (\langle z - h/2\rangle - \langle z - h_{N+2}\rangle)\phi_x(x, y, t) + \langle z - h_{N+2}\rangle\gamma_x(x, y, t) \quad (1)$$

$$v(x, y, z, t) = v_0(x, y, t) + (z - \langle z - h/2\rangle)\theta_y(x, y, t) + (\langle z - h/2\rangle - \langle z - h_{N+2}\rangle)\phi_y(x, y, t) + \langle z - h_{N+2}\rangle\gamma_y(x, y, t) \quad (2)$$

Note that the brackets $\langle\ \rangle$ are used to write the singularity functions, and implicit in Eqs. (1) and (2) are the three first-order shear deformation theories respectively for substrate, viscoelastic layer, and the PFRC layer. The transverse displacement $w(x, y, t)$ at any point in the overall plate is assumed to be constant through the thickness of all layers. For the ease of analysis, the generalized displacement variables are grouped into the following vectors of generalized translational $\{\boldsymbol{d}_t\}$ and rotational $\{\boldsymbol{d}_r\}$, $\{\boldsymbol{d}_{r1}\}$ variables:

$$\{\boldsymbol{d}_t\} = [u_0 \quad v_0 \quad w]^T, \qquad \{\boldsymbol{d}_r\} = [\theta_x \quad \theta_y]^T$$

$$\{\boldsymbol{d}_{r1}\} = [\phi_x \quad \phi_y \quad \gamma_x \quad \gamma_y]^T \quad (3)$$

To implement the selective integration rule for avoiding the shear locking in thin plates, the state of strain at a point in the overall

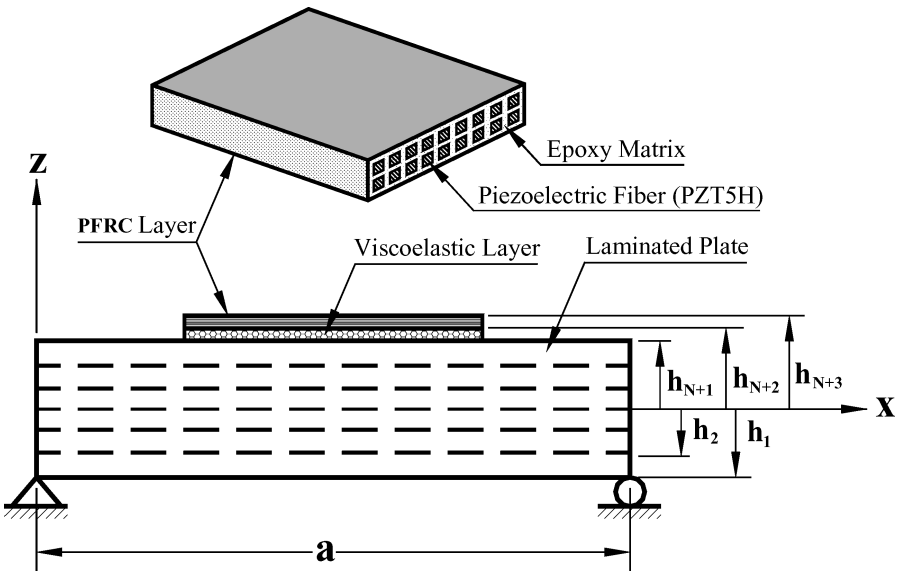

Fig. 1 Schematic representation of laminated composite plate integrated with the patches of ACLD treatment.

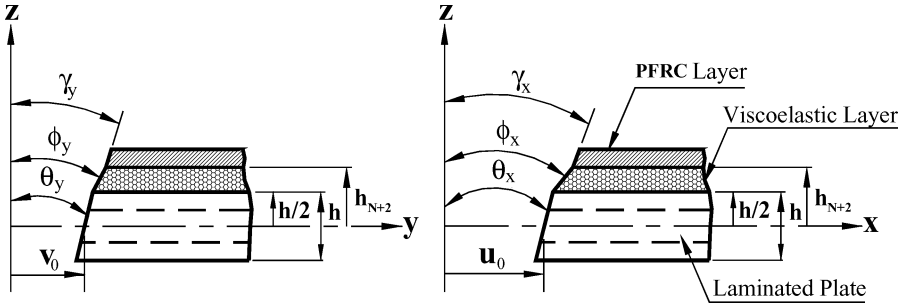

Fig. 2 Kinematics of deformation.

plate is represented by the two vectors of in-plane strains $\{\in_b\}$ and transverse strains $\{\in_s\}$, respectively, and are given by

$$\{\in_b\} = [\in_x \quad \in_y \quad \in_{xy}]^T, \qquad \{\in_s\} = [\in_{xz} \quad \in_{yz}]^T \tag{4}$$

in which $\in_x, \in_y$ are the normal strains along x and y directions, respectively; $\in_{xy}$ is the in-plane shear strain; and $\in_{xz}$ and $\in_{yz}$ are the transverse shear strains. Using the displacement field given by Eqs. (1) and (2), the linear strain-displacement relations, and Eq. (4), the vectors $\{\epsilon_b\}_c$, $\{\epsilon_b\}_v$, and $\{\epsilon_b\}_p$ defining the state of in-plane strains at any point in the substrate composite plate, viscoelastic layer, and the PFRC layer, respectively, can be expressed as

$$\{\epsilon_b\}_c = \{\epsilon_{\mathrm{bt}}\} + z\{\epsilon_{\mathrm{br}}\}$$

$$\{\epsilon_b\}_v = \{\epsilon_{\mathrm{bt}}\} + (h/2)\{\epsilon_{\mathrm{br}}\} + (z - h/2)\{\epsilon_{\mathrm{br1}}\}$$

$$\{\epsilon_b\}_p = \{\epsilon_{\mathrm{bt}}\} + (h/2)\{\epsilon_{\mathrm{br}}\} + [Z_1]\{\epsilon_{\mathrm{br2}}\} \tag{5}$$

Similarly, the vectors $\{\epsilon_s\}_c$, $\{\epsilon_s\}_v$, and $\{\epsilon_s\}_p$ defining the state of transverse shear strain at any point in the substrate plate, viscoelastic layer, and the PFRC layer, respectively, can be written as

$$\{\epsilon_s\}_c = \{\epsilon_{\mathrm{st}}\} + \{\epsilon_{\mathrm{sr}}\}, \qquad \{\epsilon_s\}_v = \{\epsilon_{\mathrm{st}}\} + \{\epsilon_{\mathrm{sr1}}\}$$

$$\{\epsilon_s\}_p = \{\epsilon_{\mathrm{st}}\} + \{\epsilon_{\mathrm{sr2}}\} \tag{6}$$

In Eqs. (5) and (6), the matrix $[\mathbf{Z}_1]$ and the various generalized vectors are given by

$$[\mathbf{Z}_1] = \begin{bmatrix} h_v & 0 & 0 & z - h_{N+2} & 0 & 0 \\ 0 & h_v & 0 & 0 & z - h_{N+2} & 0 \\ 0 & 0 & h_v & 0 & 0 & z - h_{N+2} \end{bmatrix}$$

$$\{\epsilon_{\mathrm{bt}}\} = \left[\frac{\partial u_0}{\partial x} \quad \frac{\partial v_0}{\partial y} \quad \frac{\partial u_0}{\partial y} + \frac{\partial v_0}{\partial x}\right]^T$$

$$\{\epsilon_{\mathrm{br}}\} = \left[\frac{\partial \theta_x}{\partial x} \quad \frac{\partial \theta_y}{\partial y} \quad \frac{\partial \theta_x}{\partial y} + \frac{\partial \theta_y}{\partial x}\right]^T$$

$$\{\epsilon_{\mathrm{br1}}\} = \left[\frac{\partial \phi_x}{\partial x} \quad \frac{\partial \phi_y}{\partial y} \quad \frac{\partial \phi_x}{\partial y} + \frac{\partial \phi_y}{\partial x}\right]^T$$

$$\{\epsilon_{\mathrm{br2}}\} = \left[\frac{\partial \phi_x}{\partial x} \quad \frac{\partial \phi_y}{\partial y} \quad \frac{\partial \phi_x}{\partial y} + \frac{\partial \phi_y}{\partial x} \quad \frac{\partial \gamma_x}{\partial x} \quad \frac{\partial \gamma_y}{\partial y} \quad \frac{\partial \gamma_x}{\partial y} + \frac{\partial \gamma_y}{\partial x}\right]^T$$

$$\{\epsilon_{\mathrm{st}}\} = \left[\frac{\partial w}{\partial x} \quad \frac{\partial w}{\partial y}\right]^T, \qquad \{\epsilon_{\mathrm{sr}}\} = [\theta_x \quad \theta_y]^T$$

$$\{\epsilon_{\mathrm{sr1}}\} = [\phi_x \quad \phi_y]^T, \qquad \{\epsilon_{\mathrm{sr2}}\} = [\gamma_x \quad \gamma_y]^T \tag{7}$$

Similar to the strain vectors given by Eq. (4), the in-plane stresses and the transverse shear stresses at any point in the overall plate are described by the following stress vectors:

$$\{\boldsymbol{\sigma}_b\} = [\sigma_x \quad \sigma_y \quad \sigma_{xy}]^T, \qquad \{\boldsymbol{\sigma}_s\} = [\sigma_{xz} \quad \sigma_{yz}]^T \tag{8}$$

where σ_x, σ_y are the normal stresses along x and y directions, respectively; σ_{xy} is the in-plane shear stress; and σ_{xz} and σ_{yz} are the transverse shear stresses.

The constitutive relations for the material of the PFRC layer can be expressed as[33]

$$\left\{\sigma_b^k\right\} = \left[\bar{C}_b^k\right]\left\{\epsilon_b^k\right\} - \left[\bar{e}_b^k\right]\{\boldsymbol{E}^k\}$$

$$\left\{\sigma_s^k\right\} = \left[\bar{C}_s^k\right]\left\{\epsilon_s^k\right\} - \left[\bar{e}_s^k\right]\{\boldsymbol{E}^k\} \tag{9}$$

$$\{\boldsymbol{D}^k\} = \left[\bar{e}_b^k\right]^T\left\{\epsilon_b^k\right\} + \left[\bar{e}_s^k\right]^T\left\{\epsilon_s^k\right\} + [\bar{\varepsilon}^k]\{\boldsymbol{E}^k\} \tag{10}$$

where for the kth layer, $[\bar{C}_b^k]$ and $[\bar{C}_s^k]$ are the matrices of transformed elastic coefficients referred to laminate coordinate (x, y, z) system; $[\bar{e}_b^k]$ and $[\bar{e}_s^k]$ are the matrices of corresponding transformed piezoelectric constants; $\{\boldsymbol{E}^k\}$ and $\{\boldsymbol{D}^k\}$ are the electric field and electric displacement vectors, respectively; and $[\bar{\varepsilon}^k]$ is the matrix of transformed dielectric constants. The electric field and displacement vectors appearing in Eqs. (9) and (10) are given by

$$\{\boldsymbol{E}^k\} = \left[E_x^k \quad E_y^k \quad E_z^k\right]^T, \qquad \{\boldsymbol{D}^k\} = \left[D_x^k \quad D_y^k \quad D_z^k\right]^T \tag{11}$$

in which E_x^k, E_y^k, and E_z^k are the electric field along x, y, and z axes, respectively, and D_x^k, D_y^k, and D_z^k are the corresponding electric displacements. The coefficient matrices $[\bar{C}_b^k]$, $[\bar{C}_s^k]$, $[\bar{e}_b^k]$, $[\bar{e}_s^k]$, and $[\varepsilon^k]$ of Eqs. (9) and (10) are given by

$$\left[\bar{C}_b^k\right] = \begin{bmatrix} \bar{C}_{11}^k & \bar{C}_{12}^k & \bar{C}_{16}^k \\ \bar{C}_{12}^k & \bar{C}_{22}^k & \bar{C}_{26}^k \\ \bar{C}_{16}^k & \bar{C}_{26}^k & \bar{C}_{66}^k \end{bmatrix}, \qquad \left[\bar{C}_s^k\right] = \begin{bmatrix} \bar{C}_{55}^k & \bar{C}_{45}^k \\ \bar{C}_{45}^k & \bar{C}_{44}^k \end{bmatrix}$$

$$\left[\bar{e}_b^k\right] = \begin{bmatrix} 0 & 0 & \bar{e}_{31}^k \\ 0 & 0 & \bar{e}_{32}^k \\ 0 & 0 & \bar{e}_{36}^k \end{bmatrix}, \qquad \left[\bar{e}_s^k\right] = \begin{bmatrix} \bar{e}_{15}^k & \bar{e}_{25}^k & 0 \\ \bar{e}_{14}^k & \bar{e}_{24}^k & 0 \end{bmatrix}$$

$$[\bar{\varepsilon}^k] = \begin{bmatrix} \bar{\varepsilon}_{11}^k & \bar{\varepsilon}_{12}^k & 0 \\ \bar{\varepsilon}_{12}^k & \bar{\varepsilon}_{22}^k & 0 \\ 0 & 0 & \bar{\varepsilon}_{33}^k \end{bmatrix} \tag{12}$$

Note that for the PFRC layer the value of k is to be considered as $N+2$, and if the elastic, dielectric, and piezoelectric coefficients of any layer are known with respect to its material coordinate system then the various elements of the coefficient matrices of that layer can be derived by using the standard transformation rule.[36] If the electrical terms are dropped, Eq. (9) represents the constitutive equations for each orthotropic layer ($k = 1, 2, 3, \ldots, N$) of the laminated substrate. The material of the viscoelastic layer is assumed to be linearly viscoelastic and istropic. Because the present study is concerned with the frequency response analysis, the viscoelastic material can be modeled by using the complex modulus approach, which is a frequency-domain-based model. In the complex modulus approach, the shear modulus G and Young's modulus E of the viscoelastic material are described as[19–26]

$$G = G'(1 + i\eta), \qquad E = 2G(1 + \nu) \tag{13}$$

in which G' is the storage modulus, ν is the Poisson's ratio, and η is the loss factor at a particular operating temperature and frequency. Accordingly, the elastic coefficient matrix $[C^{N+1}]$ of the viscoelastic material derived by using Eq. (13) turns out to be complex, and in the absence of electrical terms Eq. (9) also represents the constitutive relation of the viscoelastic material.[19–26]

The total potential energy T_p and the kinetic energy T_k of the plate coupled with the patches of ACLD treatment can be written as[37]

$$T_p = \frac{1}{2}\left[\sum_{k=1}^{N+2}\int_\Omega \left(\left\{\epsilon_b^k\right\}^T\left\{\sigma_b^k\right\} + \left\{\epsilon_s^k\right\}^T\left\{\sigma_s^k\right\}\right)\mathrm{d}\Omega - \int_\Omega \{E^{N+2}\}\{D^{N+2}\}\,\mathrm{d}\Omega\right] - \int_A \{d\}^T\{\boldsymbol{f}\}\,\mathrm{d}A \tag{14}$$

$$T_k = \frac{1}{2}\left[\sum_{k=1}^{N+2}\int_\Omega \rho^k(\dot{u}^2 + \dot{v}^2 + \dot{w}^2)\,\mathrm{d}\Omega\right] \tag{15}$$

in which $\{\boldsymbol{f}\}$ is the externally applied surface traction vector acting over a surface area A, Ω represents the volume of the concerned domain, and ρ^k is the mass density of the kth layer in concern. The

overall plate is discretized by eight noded isoparametric quadrilateral elements. Using Eq. (3), the generalized displacement vectors for ith ($i = 1, 2, 3, \ldots, 8$) node of an element can be expressed as

$$\{d_{\mathrm{ti}}\} = [u_{0i} \quad v_{0i} \quad w_i]^T, \qquad \{d_{\mathrm{ri}}\} = [\theta_{xi} \quad \theta_{yi}]^T$$
$$\{d_{r1i}\} = [\phi_{xi} \quad \phi_{yi} \quad \gamma_{xi} \quad \gamma_{yi}]^T \tag{16}$$

Thus the generalized displacement vectors at any point within the element can be written as

$$\{\boldsymbol{d}_{\mathrm{t}}\} = [N_t]\{\boldsymbol{d}_t^e\}, \qquad \{\boldsymbol{d}_r\} = [N_r]\{\boldsymbol{d}_r^e\}$$
$$\{\boldsymbol{d}_{r1}\} = [\bar{N}_r]\{\boldsymbol{d}_{r1}^e\} \tag{17}$$

wherein the nodal generalized translational displacement vector $\{\boldsymbol{d}_t^e\}$, the nodal generalized rotational vectors $\{\boldsymbol{d}_r^e\}$ and $\{\boldsymbol{d}_{r1}^e\}$, and the shape function matrices $[N_t]$, $[N_r]$, and $[\bar{N}_r]$ are

$$\{\boldsymbol{d}_t^e\} = \begin{bmatrix}\{d_{t1}\}^T & \{d_{t2}\}^T & \cdot & \cdot & \{d_{t8}\}^T\end{bmatrix}^T$$
$$\{\boldsymbol{d}_r^e\} = \begin{bmatrix}\{d_{r1}\}^T & \{d_{r2}\}^T & \cdot & \cdot & \{d_{r8}\}^T\end{bmatrix}^T$$
$$\{\boldsymbol{d}_{r1}^e\} = \begin{bmatrix}\{d_{r11}\}^T & \{d_{r12}\}^T & \cdot & \cdot & \{d_{r18}\}^T\end{bmatrix}^T$$
$$[N_t] = \begin{bmatrix}N_{t1} & N_{t2} & \cdot & \cdot & N_{t8}\end{bmatrix}$$
$$[N_r] = [N_{r1} \quad N_{r2} \quad \cdot \quad \cdot \quad N_{r8}]$$
$$[\bar{N}_r] = [\bar{N}_{r1} \quad \bar{N}_{r2} \quad \cdot \quad \cdot \quad \bar{N}_{r8}]$$
$$N_{\mathrm{ti}} = n_i I_t, \qquad N_{\mathrm{ri}} = n_i I_r \bar{N}_{\mathrm{ri}} = n_I \bar{I}_r \tag{18}$$

in which I_t, I_r, and $\bar{I}_r$ are the identity matrices of appropriate sizes and n_i is the shape function of natural coordinates associated with the ith node of the element. Using the relations given by Eqs. (5–7), the strain vectors at any point within the element can be expressed as

$$\{\epsilon_b\}_c = [B_{\mathrm{tb}}]\{\boldsymbol{d}_t^e\} + z[B_{\mathrm{rb}}]\{\boldsymbol{d}_r^e\}$$
$$\{\in_b\}_v = [B_{\mathrm{tb}}]\{\boldsymbol{d}_t^e\} + (h/2)[B_{\mathrm{rb}}]\{\boldsymbol{d}_r^e\} + (z - h/2)[B_{\mathrm{rb}}]_v\{\boldsymbol{d}_{r1}^e\}$$
$$\{\epsilon_b\}_p = [B_{\mathrm{tb}}]\{\boldsymbol{d}_t^e\} + (h/2)[B_{\mathrm{rb}}]\{\boldsymbol{d}_r^e\} + [Z_1][B_{\mathrm{rb}}]_p\{\boldsymbol{d}_{r1}^e\}$$
$$\{\in_s\}_c = [B_{\mathrm{ts}}]\{\boldsymbol{d}_t^e\} + [B_{\mathrm{rs}}]\{\boldsymbol{d}_r^e\}$$
$$\{\epsilon_s\}_v = [B_{\mathrm{ts}}]\{\boldsymbol{d}_t^e\} + [B_{\mathrm{rs}}]_v\{\boldsymbol{d}_{r1}^e\}$$
$$\{\in_s\}_p = [B_{\mathrm{ts}}]\{\boldsymbol{d}_t^e\} + [B_{\mathrm{rs}}]_p\{\boldsymbol{d}_{r1}^e\} \tag{19}$$

In Eq. (19), the nodal generalized strain-displacement matrices are given by

$$[B_{\mathrm{tb}}] = [B_{\mathrm{tb1}} \quad B_{\mathrm{tb2}} \quad \cdots \quad B_{\mathrm{tb8}}]$$
$$[B_{\mathrm{rb}}] = [B_{\mathrm{rb1}} \quad B_{\mathrm{rb2}} \quad \cdots \quad B_{\mathrm{rb8}}]$$
$$[B_{\mathrm{ts}}] = [B_{\mathrm{ts1}} \quad B_{\mathrm{ts2}} \quad \cdots \quad B_{\mathrm{ts8}}]$$
$$[B_{\mathrm{rs}}] = [B_{\mathrm{rs1}} \quad B_{\mathrm{rs2}} \quad \cdots \quad B_{\mathrm{rs8}}]$$
$$[B_{\mathrm{rb}}]_v = \begin{bmatrix}B_{\mathrm{rb1}}^v & B_{\mathrm{rb2}}^v & \cdots & B_{\mathrm{rb8}}^v\end{bmatrix}$$
$$[B_{\mathrm{rs}}]_v = \begin{bmatrix}B_{\mathrm{rs1}}^v & B_{\mathrm{rs2}}^v & \cdots & B_{\mathrm{rs8}}^v\end{bmatrix}$$
$$[B_{\mathrm{rb}}]_p = \begin{bmatrix}B_{\mathrm{rb1}}^p & B_{\mathrm{rb2}}^p & \cdots & B_{\mathrm{rb8}}^p\end{bmatrix}$$
$$[B_{\mathrm{rs}}]_p = \begin{bmatrix}B_{\mathrm{rs1}}^p & B_{\mathrm{rs2}}^p & \cdots & B_{\mathrm{rs8}}^p\end{bmatrix} \tag{20}$$

in which

$$B_{\mathrm{tbi}} = [B_{\mathrm{rbi}} \quad O], \qquad B_{\mathrm{rbi}} = \begin{bmatrix}n_{i,x} & 0\\ 0 & n_{i,y}\\ n_{i,y} & n_{i,x}\end{bmatrix}$$
$$B_{\mathrm{tsi}} = \begin{bmatrix}0 & 0 & n_{i,x}\\ 0 & 0 & n_{i,y}\end{bmatrix}, \qquad B_{\mathrm{rsi}} = \begin{bmatrix}n_i & 0\\ 0 & n_i\end{bmatrix}, \qquad n_{i,x} = \frac{\partial n_i}{\partial x}$$
$$n_{i,y} = \frac{\partial n_i}{\partial y}, \qquad B_{\mathrm{rbi}}^v = [B_{\mathrm{rbi}} \quad \tilde{O}], \qquad B_{\mathrm{rbi}}^p = \begin{bmatrix}B_{\mathrm{rbi}} & \tilde{O}\\ \tilde{O} & B_{\mathrm{rbi}}\end{bmatrix}$$
$$B_{\mathrm{rsi}}^p = [\bar{O} \quad B_{\mathrm{rsi}}], \qquad B_{\mathrm{rsi}}^v = [B_{\mathrm{rsi}} \quad \bar{O}] \tag{21}$$

wherein O, $\tilde{O}$, and $\bar{O}$ are the (3×1), (3×2), and (2×2) null matrices, respectively. The poling direction in the fibers is transverse to the fiber direction, and hence the electric field is considered to act along the thickness direction of the PFRC layer only. Thus, the electric field vector given by Eq. (11) can be written for the PFRC layer as

$$\{E^{N+2}\} = [0 \quad 0 \quad -(1/h_p)]^T V \tag{22}$$

where V is the potential difference across the thickness of the PFRC layer and spatially constant over the surface of the PFRC layer.

Substituting Eqs. (9) and (10) into Eq. (14) and then using Eqs. (19) and (22), the total potential energy T_p^e of a typical element augmented with the ACLD treatment can be written as

$$\begin{aligned}T_p^e = \tfrac{1}{2}\Big[&\{\boldsymbol{d}_t^e\}^T[K_t^e]\{\boldsymbol{d}_t^e\} + \{\boldsymbol{d}_t^e\}^T\left[K_{\mathrm{tr}}^e\right]\{\boldsymbol{d}_r^e\} + \{\boldsymbol{d}_r^e\}^T\left[K_{\mathrm{tr}}^e\right]^T\{\boldsymbol{d}_t^e\}\\ &+ \{\boldsymbol{d}_r^e\}^T\left[K_{\mathrm{rr}}^e\right]\{\boldsymbol{d}_r^e\} + \{\boldsymbol{d}_t^e\}^T\left[K_{\mathrm{tr1}}^e\right]\{\boldsymbol{d}_{r1}^e\} + \{\boldsymbol{d}_{r1}^e\}^T\left[K_{\mathrm{tr1}}^e\right]^T\{\boldsymbol{d}_t^e\}\\ &+ \{\boldsymbol{d}_r^e\}^T\left[K_{\mathrm{rr1}}^e\right]\{\boldsymbol{d}_{r1}^e\} + \{\boldsymbol{d}_{r1}^e\}^T\left[K_{\mathrm{rr1}}^e\right]^T\{\boldsymbol{d}_r^e\}\\ &+ \{\boldsymbol{d}_{r1}^e\}^T\left[K_{\mathrm{rr2}}^e\right]^T\{\boldsymbol{d}_{r1}^e\} - 2\{\boldsymbol{d}_t^e\}^T\{f_{\mathrm{tp}}^e\}V - 2\{\boldsymbol{d}_r^e\}^T\{f_{\mathrm{rp}}^e\}V\\ &- 2\{d_{r1}^e\}^T\{f_{r1p}^e\}V\Big] - \{\boldsymbol{d}_t^e\}^T\{F^e\}\end{aligned} \tag{23}$$

The elemental stiffness matrices $[K_t^e]$, $[K_{\mathrm{tr}}^e]$, $[K_{\mathrm{rr}}^e]$, $[K_{\mathrm{tr1}}^e]$, $[K_{\mathrm{rr1}}^e]$, $[K_{\mathrm{rr2}}^e]$; the elemental electroelastic coupling vectors $\{F_{\mathrm{tp}}^e\}$, $\{F_{\mathrm{rp}}^e\}$, $\{F_{\mathrm{r1p}}^e\}$; and the elemental load vector $\{\boldsymbol{F}^e\}$ appearing in Eq. (23) are given by

$$\left[K_t^e\right] = \int_0^{b_e}\int_0^{a_e}\left([B_{\mathrm{tb}}]^T[D_{\mathrm{tb}}][B_{\mathrm{tb}}] + [B_{\mathrm{ts}}]^T[D_{\mathrm{ts}}][B_{\mathrm{ts}}]\right)\mathrm{d}x\,\mathrm{d}y$$
$$\left[K_{\mathrm{tr}}^e\right] = \int_0^{b_e}\int_0^{a_e}\left([B_{\mathrm{tb}}]^T[D_{\mathrm{trb}}][B_{\mathrm{rb}}] + [B_{\mathrm{ts}}]^T[D_{\mathrm{trs}}][B_{\mathrm{rs}}]\right)\mathrm{d}x\,\mathrm{d}y$$
$$\left[K_{\mathrm{rr}}^e\right] = \int_0^{b_e}\int_0^{a_e}\left([B_{\mathrm{tb}}]^T[D_{\mathrm{rrb}}][B_{\mathrm{rb}}] + [B_{\mathrm{rs}}]^T[D_{\mathrm{rrs}}][B_{\mathrm{rs}}]\right)\mathrm{d}x\,\mathrm{d}y$$
$$\begin{aligned}\left[K_{\mathrm{tr1}}^e\right] = \int_0^{b_e}\int_0^{a_e}\Big([B_{\mathrm{tb}}]^T[D_{\mathrm{tr1b}}]_v[B_{\mathrm{tb}}]_v + [B_{\mathrm{tb}}]^T[D_{\mathrm{tr1b}}]_p[B_{\mathrm{rb}}]_p\\ + [B_{\mathrm{ts}}]^T[D_{\mathrm{trs}}]_v[B_{\mathrm{rs}}]_v + [B_{\mathrm{ts}}]^T[D_{\mathrm{trs}}]_p[B_{\mathrm{rs}}]_p\Big)\mathrm{d}x\,\mathrm{d}y\end{aligned}$$
$$\left[K_{\mathrm{rr1}}^e\right] = \int_0^{b_e}\int_0^{a_e}\left([B_{\mathrm{rb}}]^T[D_{\mathrm{rr1b}}]_v[B_{\mathrm{rb}}]_v + [B_{\mathrm{rb}}]^T[D_{\mathrm{rr1b}}]_p[B_{\mathrm{rb}}]_p\,\mathrm{d}x\,\mathrm{d}y\right.$$
$$\begin{aligned}\left[K_{\mathrm{rr2}}^e\right] = \int_0^{b_e}\int_0^{a_e}\Big([B_{\mathrm{rb}}]_v^T[D_{\mathrm{rr2b}}]_v[B_{\mathrm{rb}}]_v + [B_{\mathrm{rb}}]_p^T[D_{\mathrm{rr2b}}]_p[B_{\mathrm{rb}}]_p\\ + [B_{\mathrm{rs}}]_v^T[D_{\mathrm{rrs}}]_v[B_{\mathrm{rs}}]_v + [B_{\mathrm{rs}}]_p^T[D_{\mathrm{rrs}}]_p[B_{\mathrm{rs}}]_p\Big)\mathrm{d}x\,\mathrm{d}y\end{aligned}$$
$$\left\{f_{\mathrm{tp}}^e\right\} = \int_0^{b_e}\int_0^{a_e}\left([B_{\mathrm{tb}}]^T\{F_{\mathrm{tb}}\}_p + [B_{\mathrm{ts}}]^T\{F_{\mathrm{ts}}\}_p\right)\mathrm{d}x\,\mathrm{d}y$$
$$\left\{f_{\mathrm{rp}}^e\right\} = \int_0^{b_e}\int_0^{a_e}[B_{\mathrm{rb}}]^T\{F_{\mathrm{rb}}\}_p\,\mathrm{d}x\,\mathrm{d}y$$

$$\left\{f^e_{\mathrm{r1p}}\right\} = \int_0^{b_e}\int_0^{a_e}\left([B_{\mathrm{rb}}]^T_p\{F_{r1b}\}_p + [B_{\mathrm{rs}}]^T_p\{F_{r1s}\}_p\right)\mathrm{d}x\,\mathrm{d}y$$

$$\{\boldsymbol{F}^e\} = \int_0^{b_e}\int_0^{a_e}[N_t]^T\{f\}\,\mathrm{d}x\,\mathrm{d}y$$

wherein a_e and b_e are the length and width of the element in consideration and the various rigidity matrices originated in the elemental matrices are

$$[D_{\mathrm{tb}}] = \sum_{k=1}^{N+2}\int_{h_k}^{h_{k+1}}\left[\bar{C}^k_b\right]\mathrm{d}z$$

$$[D_{\mathrm{ts}}] = \sum_{k=1}^{N+2}\int_{h_k}^{h_{k+1}}\left[\bar{C}^k_s\right]\mathrm{d}z$$

$$[D_{\mathrm{trb}}] = \sum_{k=1}^{N}\int_{h_k}^{h_{k+1}} z\left[\bar{C}^k_b\right]\mathrm{d}z + \sum_{k=N+1}^{N+2}\int_{h_k}^{h_{k+1}}\frac{h}{2}\left[\bar{C}^k_b\right]\mathrm{d}z$$

$$[D_{\mathrm{trs}}] = \sum_{k=1}^{N}\int_{h_k}^{h_{k+1}}\left[\bar{C}^k_s\right]\mathrm{d}z$$

$$[D_{\mathrm{trs}}]_v = \int_{h_{N+1}}^{h_{N+2}}\left[\bar{C}^{N+1}_s\right]\mathrm{d}z$$

$$[D_{\mathrm{rrb}}] = \sum_{k=1}^{N}\int_{h_k}^{h_{k+1}} z^2\left[\bar{C}^k_b\right]\mathrm{d}z + \sum_{k=N+1}^{N+2}\int_{h_k}^{h_{k+1}}\frac{h^2}{4}\left[\bar{C}^k_b\right]\mathrm{d}z$$

$$[D_{\mathrm{tr1}b}]_v = \int_{h_{N+1}}^{h_{N+2}}\left(z-\frac{h}{2}\right)\left[\bar{C}^{N+1}_b\right]\mathrm{d}z$$

$$[D_{\mathrm{tr1}b}]_p = \int_{h_{N+2}}^{h_{N+3}}\left[\bar{C}^{N+2}_b\right][Z_1]\,\mathrm{d}z$$

$$[D_{\mathrm{trs}}]_p = \int_{h_{N+2}}^{h_{N+3}}\left[\bar{C}^{N+2}_s\right]\mathrm{d}z$$

$$[D_{\mathrm{rrs}}] = [D_{\mathrm{trs}}], \qquad [D_{\mathrm{rrs}}]_p = [D_{\mathrm{trs}}]_p, \qquad [D_{\mathrm{rrs}}]_v = [D_{\mathrm{trs}}]^v$$

$$[D_{\mathrm{trr1}b}]_v = \int_{h_{N+1}}^{h_{N+2}}\frac{h}{2}\left(z-\frac{h}{2}\right)\left[\bar{C}^{N+1}_b\right]\mathrm{d}z$$

$$[D_{\mathrm{trr1}b}]_p = \int_{h_{N+2}}^{h_{N+3}}\frac{h}{2}\left[\bar{C}^{N+2}_b\right][Z_1]\,\mathrm{d}z$$

$$[D_{\mathrm{trr2b}}]_v = \int_{h_{N+1}}^{h_{N+2}}\left(z-\frac{h}{2}\right)^2\left[\bar{C}^{N+1}_b\right]\mathrm{d}z$$

$$[D_{\mathrm{trr2b}}]_p = \int_{h_{N+2}}^{h_{N+3}}[Z_1]^T\left[\bar{C}^{N+2}_b\right][Z_1]\,\mathrm{d}z$$

$$\{F_{\mathrm{tb}}\}_p = \int_{h_{N+1}}^{h_{N+2}}\left[\bar{e}^{N+2}_b\right]\{\bar{E}\}\,\mathrm{d}z$$

$$\{F_{\mathrm{ts}}\}_p = \int_{h_{N+1}}^{h_{N+2}}\left[\bar{e}^{N+2}_s\right][\bar{E}]\,\mathrm{d}z$$

$$\{F_{\mathrm{rb}}\}_p = \int_{h_{N+1}}^{h_{N+2}}\left(\frac{h}{2}\right)\left[\bar{e}^{N+2}_b\right]\{\bar{E}\}\,\mathrm{d}z$$

$$\{F_{r1b}\}_p = \int_{h_{N+1}}^{h_{N+2}}[Z_1]^T\left[\bar{e}^{N+2}_b\right]\{\bar{E}\}\,\mathrm{d}z, \qquad \{F_{r1s}\}_p = \{F_{\mathrm{ts}}\}_p$$

Note that as the elastic coefficient matrices of the viscoelastic material are complex, the elemental stiffness matrices are complex for an element augmented with the ACLD treatment. Using Eq. (17) in Eq. (15), the kinetic energy T^e_k of the element can be obtained as

$$T^e_k = \tfrac{1}{2}\left\{\dot{\boldsymbol{d}}^e_t\right\}^T[M^e]\left\{\dot{\boldsymbol{d}}^e_t\right\} \tag{24}$$

in which

$$[M^e] = \int_0^{a_e}\int_0^{b_e}\bar{m}[N_t]^T[N_t]\,\mathrm{d}x\,\mathrm{d}y$$

$$\bar{m} = \sum_{k=1}^{N}\rho^k(h_{k+1}-h_k) + \rho^{N+1}h_v + \rho^{N+2}h_p$$

The rotary inertia of the overall plate has been neglected to estimate the kinetic energy of the overall plate as the substrate plates considered here are very thin. Applying the principle of virtual work,[24] the following governing equations of an element are obtained:

$$[M^e]\left\{\ddot{\boldsymbol{d}}^e_t\right\} + \left[K^e_t\right]\left\{\boldsymbol{d}^e_t\right\} + \left[K^e_{\mathrm{tr}}\right]\left\{\boldsymbol{d}^e_r\right\} + [K^e_{\mathrm{tr1}}]\left\{\boldsymbol{d}^e_{r1}\right\} = \left\{f^e_{\mathrm{tp}}\right\}V + \{\boldsymbol{F}^e\} \tag{25}$$

$$\left[K^e_{\mathrm{tr}}\right]^T\left\{\boldsymbol{d}^e_t\right\} + \left[K^e_{\mathrm{rr}}\right]\left\{\boldsymbol{d}^e_r\right\} + \left[K^e_{\mathrm{rr1}}\right]\left\{\boldsymbol{d}^e_{r1}\right\} = \left\{f^e_{\mathrm{rp}}\right\}V \tag{26}$$

$$\left[K^e_{\mathrm{tr1}}\right]^T\left\{\boldsymbol{d}^e_t\right\} + \left[K^e_{\mathrm{rr1}}\right]\left\{\boldsymbol{d}^e_r\right\} + \left[K^e_{\mathrm{rr2}}\right]\left\{\boldsymbol{d}^e_{r1}\right\} = \left\{f^e_{\mathrm{r1p}}\right\}V \tag{27}$$

Equations (25) and (26) also represent the formulation of an element without integration with the ACLD treatment. In that case, the elemental stiffness matrices $[K^e_{\mathrm{tr1}}]$, $[K^e_{\mathrm{rr1}}]$, $[K^e_{\mathrm{rr2}}]$ and the electroelastic coupling matrices $\{\boldsymbol{F}^e_{\mathrm{tp}}\}$, $\{\boldsymbol{F}^e_{\mathrm{rp}}\}$, $\{\boldsymbol{F}^e_{r1p}\}$ turn out to be the null matrices, and the other elemental stiffness matrices become real. The method of formulation leads to the derivation of the relations between the nodal rotational degrees of freedom $\{\boldsymbol{d}^e_{r1}\}$ and the remaining degrees of freedom $\{\boldsymbol{d}^e_t\}$ and $\{\boldsymbol{d}^e_r\}$ of an element integrated with the patch of ACLD treatment as manifested by Eq. (27). Also, the edge boundary conditions will be considered as simply supported for the boundaries of the substrate composite plates only. Because the rotational degrees of freedom $\{\boldsymbol{d}^e_{r1}\}$ are not explicitly involved with the edges of the substrate plate, these degrees of freedom are condensed at the elemental level yielding the set of elemental equations of motion in terms of the nodal degrees of freedom $\{\boldsymbol{d}^e_t\}$ and $\{\boldsymbol{d}^e_r\}$ as follows:

$$[M^e]\left\{\ddot{\boldsymbol{d}}^e_t\right\} + \left[K^e_{\mathrm{tt}}\right]\left\{\boldsymbol{d}^e_t\right\} + \left[K^e_{\mathrm{trac}}\right]\left\{\boldsymbol{d}^e_r\right\} = \left\{\boldsymbol{F}^e_{\mathrm{tp}}\right\}V + \{\boldsymbol{F}^e\} \tag{28}$$

$$\left[K^e_{\mathrm{trac}}\right]^T\left\{\boldsymbol{d}^e_t\right\} + \left[K^e_{\mathrm{rrac}}\right]\left\{\boldsymbol{d}^e_r\right\} = \left\{\boldsymbol{F}^e_{\mathrm{rp}}\right\}V \tag{29}$$

in which the augmented elemental matrices are given by

$$\left[K^e_{\mathrm{tt}}\right] = \left[K^e_t\right] - \left[K^e_{\mathrm{tr1}}\right]\left[K^e_{\mathrm{rr2}}\right]^{-1}\left[K^e_{\mathrm{tr1}}\right]^T$$

$$\left[K^e_{\mathrm{trac}}\right] = \left[K^e_{\mathrm{tr}}\right] - \left[K^e_{\mathrm{tr1}}\right]\left[K^e_{\mathrm{rr2}}\right]^{-1}\left[K^e_{\mathrm{rr1}}\right]^T$$

$$\left\{\boldsymbol{F}^e_{\mathrm{tp}}\right\} = \left\{f^e_{\mathrm{tp}}\right\} - \left[K^e_{\mathrm{tr1}}\right]\left[K^e_{\mathrm{rr2}}\right]^{-1}\left\{\boldsymbol{f}^e_{r1p}\right\}$$

$$\left\{\boldsymbol{F}^e_{\mathrm{rp}}\right\} = \left\{f^e_{\mathrm{rp}}\right\} - \left[K^e_{\mathrm{rr1}}\right]\left[K^e_{\mathrm{rr2}}\right]^{-1}\left\{f^e_{r1p}\right\}$$

The elemental equations of motion can be assembled to form the global equations of motion in such a manner that each patch can be activated separately as follows:

$$[M]\{\ddot{X}\} + [K_{\mathrm{tt}}]\{X\} + [K_{\mathrm{tr}}]\{X_r\} = \sum_{j=1}^{m}\left\{F^j_{\mathrm{tp}}\right\}V^j + \{\boldsymbol{F}\} \tag{30}$$

$$[K_{\mathrm{tr}}]^T\{X\} + [K_{\mathrm{rr}}]\{X_r\} = \sum_{j=1}^{m}\left\{F^j_{\mathrm{rp}}\right\}V^j \tag{31}$$

where $[M]$ is the global mass matrix; $[K_{tt}]$, $[K_{tr}]$, $[K_{rr}]$ are the global stiffness matrices; $\{X\}$ and $\{X_r\}$ are the global nodal translational and rotational degrees of freedom; $\{F_{tp}^j\}$ and $\{F_{rp}^j\}$ are the global electroelastic coupling matrices corresponding to the jth patch; V^j is the voltage applied to this patch; m is the number of patches; and $\{\boldsymbol{F}\}$ is global nodal force vector. After invoking the boundary conditions, the global rotational degrees of freedom can be condensed to obtain the global open-loop equations of motion in terms of translational degrees of freedom only as follows:

$$[M]\{\ddot{X}\} + [K^*]\{X\} = \sum_{j=1}^{m} \left\{F_p^j\right\} V^j + \{\boldsymbol{F}\} \tag{32}$$

in which

$$[K^*] = [K_{tt}] - [K_{tr}][K_{rr}]^{-1}[K_{tr}]^T$$

$$\left\{F_p^j\right\} = \left\{F_{tp}^j\right\} - [K_{tr}][K_{rr}]^{-1}\left\{F_{rp}^j\right\}$$

Recalling that the elemental stiffness matrix for an element augmented with the ACLD treatment is complex, one can realize that the global stiffness matrix $[K^*]$ is a complex matrix, and its imaginary part is responsible for contribution to the dissipation of energy.[19–26] Hence, when the piezoelectric constraining layer is not subjected to any voltage (i.e., $V = 0$), the equations of motion given by Eq. (32) represent the modeling of the passive constrained layer damping of the substrate plates.[19–26]

III. Closed-Loop Model

To supply the control voltage for activating the patches of the ACLD treatment, a simple velocity feedback control law has been employed. According to this law, the control voltage for each patch can be expressed in terms of the derivatives of the global nodal degrees of freedom as follows:

$$V^j = -K_d^j \dot{w} = -K_d^j [\boldsymbol{N}^j]\{\dot{X}\} \tag{33}$$

in which K_d^j is the control gain for the jth patch and $[\boldsymbol{N}^j]$ is a unit vector defining the location of sensing the velocity signal that will be fed back to this patch. Finally substituting Eq. (33) into Eq. (32), the equations of motion governing the closed-loop dynamics of the substrates activated by the patches of ACLD treatments are obtained as follows:

$$[M]\{\ddot{X}\} + [C_d]\{\dot{X}\} + [K^*]\{X\} = \{F\} \tag{34}$$

wherein

$$[C_d] = \sum_{j=1}^{m} K_d^j \left\{F_p^j\right\}[N^j]$$

is the active damping matrix. Note that if the control gains are zero, Eq. (34) reduces to Eq. (32) representing the passive constrained layer damping of the substrates. Thus for nonzero values of the control gain, Eq. (34) represents the modeling of the substrate plates undergoing both passive and active damping simultaneously, which is the essence of the active constrained layer damping treatment.

IV. Numerical Results

In this section, the numerical results are evaluated using the finite element model derived in the preceding section. Both cross-ply and angle-ply thin square substrates integrated with two patches of ACLD treatment are considered as the numerical examples. The locations of the patches have been selected on the basis of a recent study[26] on optimal placement of ACLD treatments such that dissipation of energy corresponding to first two modes (1,1) and (1,2) becomes maximum and are shown in Fig. 3. Unless otherwise mentioned, the thicknesses of the PFRC layer, the viscoelastic layer, and the piezoelectric fiber orientation in the PFRC layer are considered as 250 μm, 50.8 μm, and 0 deg, respectively. The thickness of each layer of the substrate plates is assumed as 1 mm. The materials of the piezoelectric fiber and the matrix of the PFRC layer are PZT5H and epoxy, respectively. Considering 40% fiber volume fraction, the elastic and piezoelectric properties of the PFRC layer with respect to its material coordinate system are evaluated by the micromechanics model developed by the authors[33] and are presented in Tables 1 and 2, respectively. Table 1 also contains the material properties of the orthotropic layers of the substrates. The value of the piezoelectric coefficient e_{32} of the PFRC material used in this study with respect to the material coordinate system is much lower than that of e_{31} as shown in Table 2, and hence this piezoelectric coefficient has not been considered for computing the numerical results. But the value of the transformed piezoelectric constant $\bar{e}_{32}^{N+2}$ will be appreciable when the fiber orientation in the PFRC is other than 0 deg and has been considered here to compute the numerical results through the use of the constitutive relations (9) and (10), which are based on the transformed coefficient matrices given by Eq. (12). Because of the formulation by using first-order shear deformation theories, the coefficient e_{33} of the PFRC is not useful here, and also, as the electric fields in the x and y directions are not considered in this study, the computation of numerical results does not require the other piezoelectric coefficients e_{15} and e_{24} of the PFRC material considered here. At an ambient temperature, the loss factor of the viscoelastic layer considered for numerical results remains invariant[25] within the frequency range of interest (0–600 Hz) and considering this ambient temperature the values of the complex shear modulus, the Poisson's ratio, and the density of the viscoelastic layer are used as $20(1+i)$ MPa, 0.49 and 1140 kg/m^3, respectively.[25] The following simply supported boundary conditions[36] are used for the cross-ply substrates to evaluate the numerical results:

$$v_0 = w = \theta_y = 0 \qquad \text{at} \qquad x = 0, a$$

$$u_0 = w = \theta_x = 0 \qquad \text{at} \qquad y = 0, b$$

Table 1 Elastic constants of the PFRC[33] and substrate layers[38]

Material	C_{11}, GPa	C_{12}, GPa	C_{22}, GPa	C_{44}, GPa	C_{55}, GPa	C_{66}, GPa	ρ, kg/m^3
PFRC	32.6	4.3	7.2	1.05	1.29	1.29	3640
Substrate layers	172.93	1.73	6.92	1.15	2.87	3.45	1600

Table 2 Piezoelectric properties of the PFRC layer[33]

Coefficient	Value
e_{31}, C/m^2	-6.76
e_{32}, C/m^2	-0.076
ε_{11}, F/m	0.037×10^{-9}
ε_{22}, F/m	10.46×10^{-9}
ε_{33}, F/m	10.46×10^{-9}

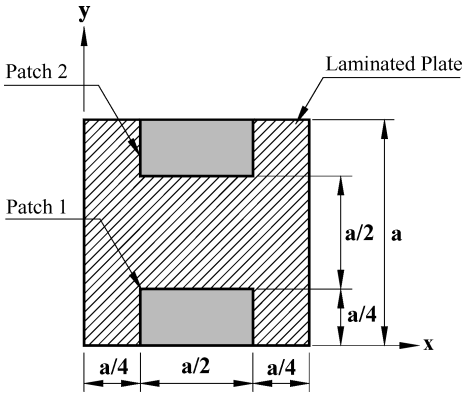

Fig. 3 Schematic representation of the locations of the patches on the top surface of the substrate.

Table 3 Fundamental natural frequencies (ϖ) of symmetric cross-ply (0/90 deg/90 deg/0) square substrates with negligible thickness of PFRC layer

Source	$a/h = 10$	$a/h = 20$	$a/h = 100$
Present FEM	15.058	17.639	18.831
Analytical[38]	15.061	17.641	18.835

Table 4 Fundamental natural frequencies (ϖ) of antisymmetric cross-ply (0 deg/90 deg/0 deg/90 deg/·/·/·) square substrates with negligible thickness of PFRC layer

	$a/h = 10$		$a/h = 20$		$a/h = 100$	
Source	$N = 2$	$N = 8$	$N = 2$	$N = 8$	$N = 2$	$N = 8$
Present FEM	8.899	12.538	9.492	14.218	9.692	14.915
Analytical[38]	8.925	12.565	9.495	14.229	9.688	14.912

Table 5 Fundamental natural frequencies (ϖ) of antisymmetric angle-ply ($-\theta/\theta/-\theta/\theta/\cdot/\cdot/\cdot$) square substrates with negligible thickness of PFRC layer

		$\theta = 5$ deg		$\theta = 30$ deg		$\theta = 45$ deg	
a/h	Source	$N = 2$	$N = 6$	$N = 2$	$N = 6$	$N = 2$	$N = 6$
10	Present FEM	14.187	14.786	12.795	18.092	13.186	18.899
	Analytical[38]	14.226	14.841	12.871	18.126	13.259	18.953
20	Present FEM	16.643	17.569	13.832	21.641	14.213	22.815
	Analytical[38]	16.657	17.618	13.847	21.650	14.233	22.867
100	Present FEM	17.772	18.928	14.217	23.286	14.613	24.726
	Analytical[38]	17.781	18.935	14.223	23.295	14.621	24.740

whereas those for the angle-ply substrate are considered as[36]

$$u_0 = w = \theta_y = 0 \qquad \text{at} \qquad x = 0, a$$

$$v_0 = w = \theta_x = 0 \qquad \text{at} \qquad y = 0, b$$

To verify the validity of the present finite element model (FEM), first the natural frequencies of the substrates integrated with the inactivated patches of ACLD treatment of negligible thickness are computed and subsequently compared with the existing analytical results[38] of identical substrates without integrated with the patches. A nondimensional frequency parameter ϖ has been used for presenting the fundamental natural frequencies of the plates and is defined as

$$\varpi = (\omega a^2/h)\sqrt{\rho/E_T} \tag{35}$$

in which ω epresents the natural frequencies of the overall plates and ρ and E_T are the density and transverse Young's modulus of the orthotropic layers of the substrates, respectively. Tables 3–5 demonstrate this comparison of the fundamental natural frequencies of symmetric cross-ply, antisymmetric cross-ply, and antisymmetric angle-ply substrates, respectively. It can be observed from these tables that the results are in excellent agreement, validating the model derived here. Next, using this FEM, the natural frequencies, passive and active damping ratios of an aluminum plate integrated with a patch of ACLD treatment as considered by Baz and Ro[20] have been determined and are compared the predictions by Baz and Ro[20] as shown in Table 6. As can be noticed from this table, the excellent agreement of the results verifies the modeling method of the ACLD treatment presented here.

The open-loop and closed-loop behavior of the substrates are studied by the frequency response functions evaluated at a point $(a/2, a/4, h/2)$ on the top of the substrates. A time-harmonic point force is considered to act at a point $(a/4, a/4, h/2)$ to excite the first few modes of the substrates. The control voltage supplied to the patch number 1 is negatively proportional to the velocity at the point $(a/2, a/4, h/2)$ and that supplied to the patch number 2 is negatively proportional to the velocity at the point $(a/2, 3a/4, h/2)$. The control gain is chosen arbitrarily such that the first few modes

Table 6 Comparison of the dynamical characteristics of a plate/ACLD system

	Natural frequency, Hz		Open-loop damping ratio		Closed-loop damping ratio
Source	1st mode	2nd mode	1st mode	2nd mode	1st mode
Present FEM	5.72	24.97	0.0316	0.0292	0.064
Baz and Ro[20]	5.76	24.99	0.0314	0.0286	0.065

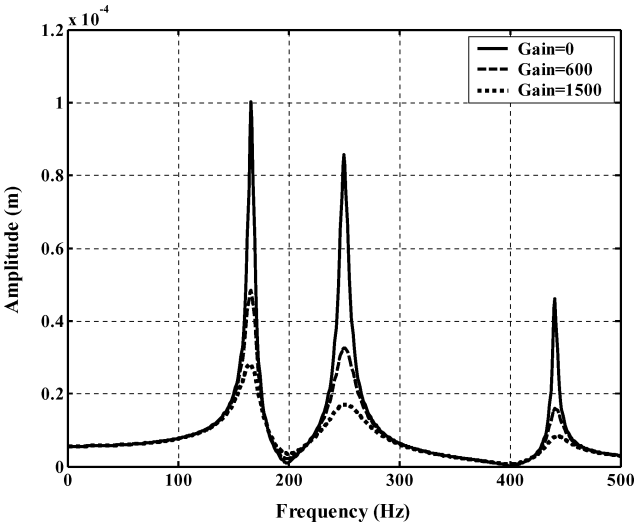

Fig. 4 Frequency response of symmetric cross-ply (0 deg/90 deg/0 deg) square substrate plate ($a/h = 100$).

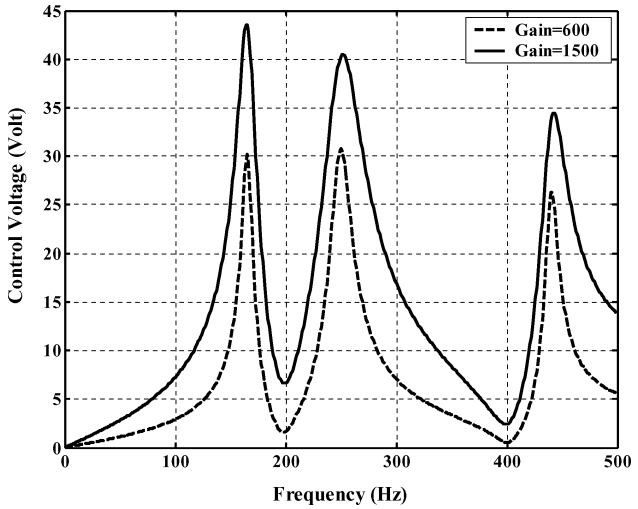

Fig. 5 Control voltage for active constrained layer damping of symmetric cross-ply (0 deg/90 deg/0 deg) square substrate plate ($a/h = 100$).

are efficiently controlled. Figure 4 illustrates the frequency response functions for symmetric square cross-ply (0 deg/90 deg/0 deg) substrate plate with $a/h = 100$. Displayed in the figure are the responses when the patches are passive (Gain = 0) and active with different gains. It is evident from the figure that the active patches significantly improves the damping characteristics of the plate for both modes over the passive damping (Gain = 0). As the gain increases, attenuation of the amplitudes of vibration also increases. The control voltages corresponding to the gains used are quite nominal, as shown in Fig. 5. The frequency response function at the same point of a thin $(a/h = 100)$ antisymmetric angle-ply substrate (−45 deg/45 deg/−45 deg/45 deg) has been shown in Figs. 6 and 7 demonstrates the corresponding control voltage. In this case also, the patches efficiently attenuate the amplitudes of vibrations

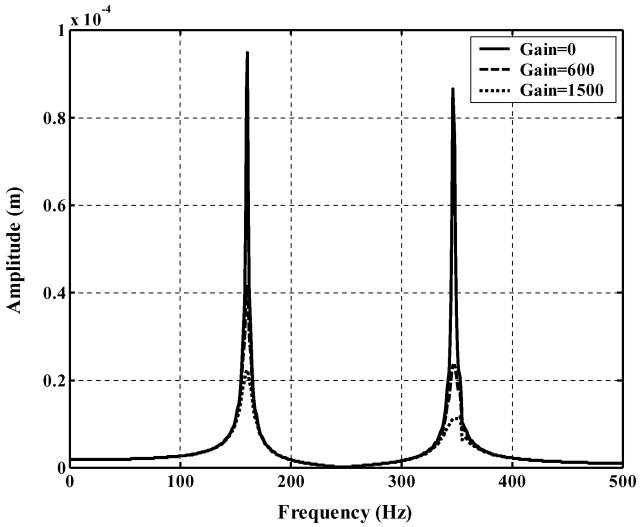

Fig. 6 Frequency response of antisymmetric angle-ply (−45 deg/45 deg/−45 deg/45 deg) square substrate plate ($a/h = 100$).

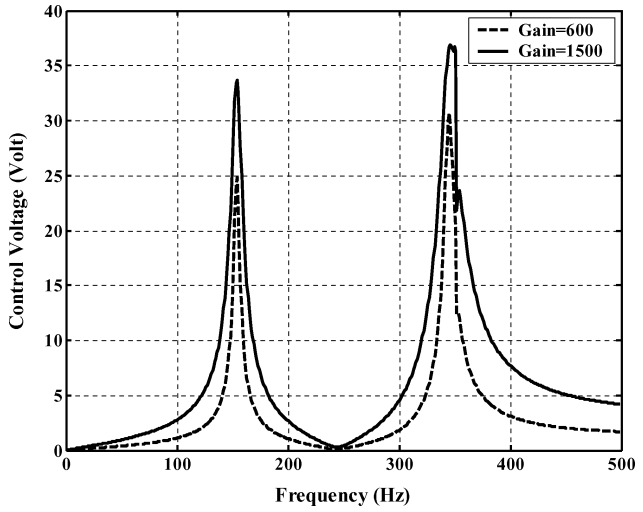

Fig. 7 Control voltage for active constrained layer damping of antisymmetric angle-ply (−45 deg/45 deg/−45 deg/45 deg) square substrate plate ($a/h = 100$).

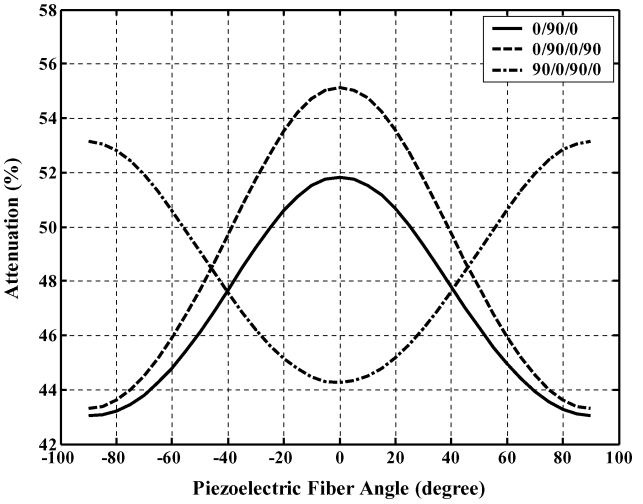

Fig. 8 Variation of control authority of the patches with respect to the piezoelectric fiber angle ψ in the PFRC layer for controlling first mode of vibration of cross-ply square plates ($a/h = 100$).

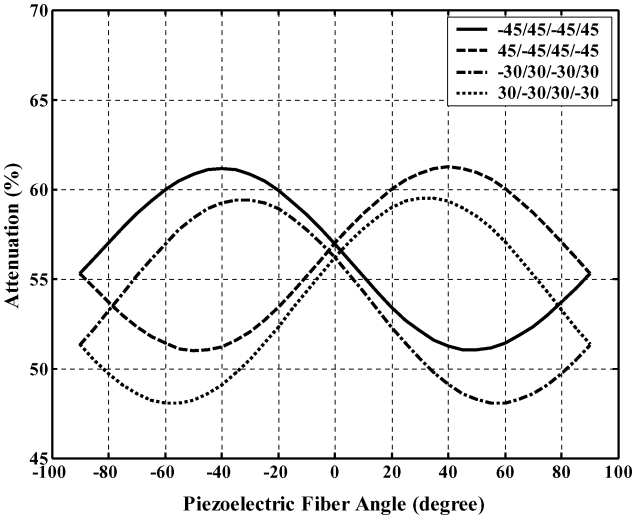

Fig. 9 Variation of control authority of the patches with respect to the piezoelectric fiber angle ψ in the PFRC layer for controlling first mode of vibration of antisymmetric angle-ply square plates ($a/h = 100$).

enhancing the damping characteristics of the plate with low control voltage.

The important aspect of this finite element analysis is to investigate the effect of variation of fiber orientation ψ in the PFRC layer on its capability of enhancing the damping characteristics of the substrates. For this using a particular value of control gain ($K_d^j = 600$) for both the patches, the percentage attenuations of vibrations are computed with different values of ψ considering various cases of cross-ply and angle-ply substrates. Figure 8 demonstrates that for controlling the first mode of vibration of thin ($a/h = 100$) symmetric cross-ply (0 deg/90 deg/0 deg) plate the maximum attenuation is achieved when $\psi = 0$ deg, whereas for thin ($a/h = 100$) four-layered antisymmetric cross-ply substrates the control authority of the PFRC layer becomes maximum when $\psi = 0$ or 90 deg according as the fiber orientation in the top layer of the substrate plate being treated with the patches be 90 or 0 deg, respectively. Although not shown here, the results remain same even if the number of layers changes. The first mode (1,1) of all of the substrate plates is a bending mode. Hence, in case of symmetric cross-ply (0 deg/90 deg/0 deg) plate in which the coupling of stretching and bending is absent the maximum attenuation is achieved when $\psi = 0$ deg for which $\bar{e}_{31}^{N+2}$ is maximum. In case of antisymmetric cross-ply plates, the coupling of bending and stretching should be reduced to achieve better control of bending mode. With a very low value of Young's modulus, the viscoelastic layer does not contribute appreciably to the stretching-bending coupling stiffness of the overall plate. It can be shown that to reduce the magnitude of stretching-bending coupling stiffness if the fiber orientation in the top layer of the antisymmetric cross-ply plate is 90 deg then the fiber orientation in the PFRC layer should be 0 deg or vice versa. Figure 8 corroborates this phenomena while achieving maximum attenuation in case of antisymmetric cross-ply plates. Figure 8 also shows that the attenuating capability of the patches does not depend on the sign of the fiber orientation ψ in the PFRC layer for controlling the first mode of vibration. This can be attributed to the fact that the values of the transformed elastic constants $\bar{C}_{16}^k$ and $\bar{C}_{26}^k$ are zero for the orthotropic layers of the symmetric cross-ply laminates resulting in no sign-sensitive coupling between bending and in-plane twist. The effect of variations of fiber orientation in the PFRC layer on the damping of first mode of vibration of antisymmetric angle-ply $(-\theta/\theta/-\theta/\theta/\cdots)$ substrate plates has been studied for different values of fiber angle θ in the orthotropic layers of the substrates. Figure 9 demonstrates this effect for the specific cases of four-layered ($N = 4$) substrates when $\theta = 45$ or -45 deg and 30 or -30 deg. It can be observed from this figure that unlike the cross-ply plates the capability of the patches is sensitive to the sign of the piezoelectric fiber angle ψ and is also

true for other angle-ply substrates with different number of layers not shown here. This might be caused by the fact that the transformed elastic constants $\bar{C}^k_{16}$ and $\bar{C}^k_{26}$ are sensitive to the sign of the fiber orientation in the orthotropic layers of the angle-ply substrate plates resulting in sign sensitive coupling stiffness between bending and in-plane twist. The values of the piezoelectric fiber angle ψ for which the attenuating capability of the patches becomes maximum to control the first mode of vibration have been determined for different antisymmetric angle-ply plates with different number of layers and are listed in Table 7. It can be observed from this table that the piezoelectric fiber angle varies with the number of orthotropic layers present in the antisymmetric angle-ply plates to maximize the control authority of the patches. It can also be noticed from Table 7 and Fig. 9 that the sign of this piezoelectric fiber angle in the PFRC layer is opposite to that of the orthotropic layer of the substrate being integrated with the patches. For controlling the second mode of vibration, the capability of the PFRC layer also varies with the fiber angle in the PFRC layer. For both antisymmetric cross-ply and angle-ply substrate plates, maximum attenuation of second mode of vibration will be achieved by the active patches if the fiber angle in the PFRC layer is 90 deg as shown in Figs. 10 and 11 for some specific cases.

Table 7 Piezoelectric fiber angle for achieving maximum control authority of the patches to control the fundamental mode of vibration of antisymmetric angle-ply ($-\theta/\theta/-\theta/\theta/\cdot/\cdot/\cdot$) square plates

	ψ		
θ, deg	$N = 2$, deg	$N = 4$, deg	$N = 6$, deg
± 15	∓ 24	∓ 27	∓ 28
± 30	∓ 26	∓ 33	∓ 34
± 45	∓ 31	∓ 40	∓ 41
± 60	∓ 37	∓ 46	∓ 48
± 75	∓ 47	∓ 53	∓ 54

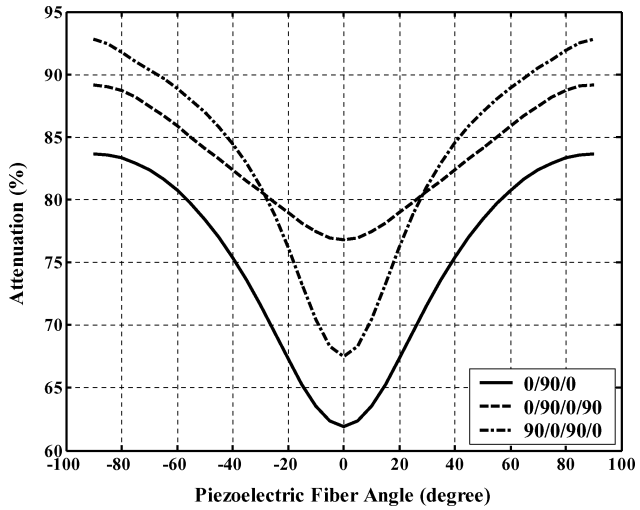

Fig. 10 Variation of control authority of patches with respect to the piezoelectric fiber angle ψ in the PFRC layer for controlling second mode of vibration of cross-ply square plates ($a/h = 100$).

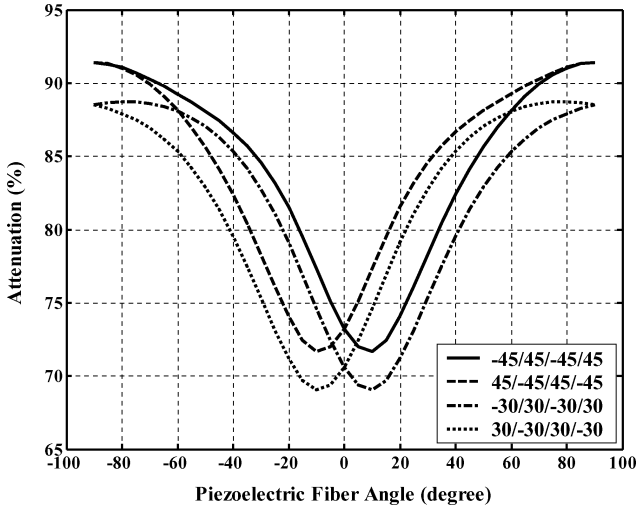

Fig. 11 Variation of control authority of patches with respect to the piezoelectric fiber angle ψ in the PFRC layer for controlling second mode of vibration of antisymmetric angle-ply square plates ($a/h = 100$).

V. Conclusions

In this paper, a finite element analysis of active constrained layer damping of thin laminated composite plates has been carried out to demonstrate the performance of piezoelectric fiber-reinforced composite (PFRC) layer as the constraining layer of active constrained layer damp (ACLD) treatment. The finite element model is based on three first-order shear deformation theories. Both symmetric/antisymmetric cross-ply and antisymmetric angle-ply laminated substrates are considered for evaluation of numerical results. Two patches are used, which are placed on the top surface of the plates such that the first two modes are efficiently controlled. The results illustrate the significant enhancement of damping characteristics of the plates over the passive damping. The analysis revealed that the fiber orientation in the PFRC layer plays a significant role in attenuating the vibration of laminated plates. In case of symmetric cross-ply plates, if the piezoelectric fiber angle in the PFRC layer be 0 and 90 deg then the capability of the patches become maximum for controlling first and second mode of vibrations, respectively. For antisymmetric cross-ply substrate plates, if the fiber angle in the orthotropic layer of the substrate being integrated with the patches be 0 or 90 deg, the fiber angle in the PFRC layer should be 90 or 0 deg to attain the maximum damping of first mode of vibration. For controlling the first mode of vibration of antisymmetric angle-ply plates, the values of the piezoelectric fiber angle in the PFRC layer have been determined to attain the maximum control authority of the patches and were found to vary with the number of layers in the substrates, and the sign of this piezoelectric fiber angle is opposite to that of the orthotropic layer of the substrate being integrated with the patches. When the fiber angle in the PFRC layer is 90 deg, the control authority of the patches becomes maximum for controlling the second mode of vibrations of both antisymmetric cross-ply and angle-ply substrate plates. It is also observed that the control authority of the PFRC layer is independent of the sign of the fiber orientation angle in the PFRC layer for cross-ply substrates, whereas it is dependent on the sign of this fiber orientation for angleply substrates.

The control of other higher modes requires the determination of optimal placement and number of the patches. This important and challenging task is a natural extension of this work and is currently under investigation.

References

[1]Bailey, T., and Hubbard, J. E., "Distributed Piezoelectric Polymer Active Vibration Control of a Cantilever Beam," *Journal of Guidance, Control, and Dynamics*, Vol. 8, No. 5, 1985, pp. 605–611.

[2]Crawley, E. F., and Luis, J. D., "Use of Piezoelectric Actuators as Elements of Intelligent Structures," *AIAA Journal*, Vol. 25, No. 10, 1987, pp. 1373–1385.

[3]Baz, A., and Poh, S., "Performance of an Active Control System with Piezoelectric Actuators," *Journal of Sound and Vibration*, Vol. 126, No. 2, 1988, pp. 327–343.

[4]Tzou, H. S., and Tseng, C. I., "Distributed Piezoelectric Sensor/Actuator Design for Dynamic Measurement/Control of Distributed Parameter Systems: A Piezoelectric Finite Element Approach," *Journal of Sound and Vibration*, Vol. 138, No. 1, 1990, pp. 17–34.

[5]Lee, C. K., Chiang, W. W., and Sulivan, O., "Piezoelectric Modal Sensor/Actuator Pairs for Critical Active Damping Vibration Control," *Journal of the Acoustical Society of America*, Vol. 90, No. 1, 1991, pp. 374–384.

[6]Hanagud, S., Obal, M. W., and Calise, A. J., "Optimal Vibration Control by the Use of Piezoceramic Sensors and Actuators," *Journal of Guidance, Control, and Dynamics*, Vol. 15, No. 5, 1992, pp. 1199–1206.

[7]Devasia, S., Tesfay, M., Paden, B., and Bayo, E. A. J., "Piezoelectric Actuator Design for Vibration Suppression: Placement and Sizing," *Journal of Guidance, Control, and Dynamics*, Vol. 16, 1993, pp. 859–864.

[8]Gu, Y., Clark, R. L., and Fuller, C. R., "Experiments on Active Control of Plate Vibration Using Piezoelectric Actuators and Polyvinylidyne Fluoride (PVDF) Modal Sensors," *Journal of Vibrations and Acoustics*, Vol. 116, No. 3, 1994, pp. 303–308.

[9]Zhou, R. C., Lai, Z., Xue, D. Y., Huang, J. K., and Mei, C., "Suppression of Nonlinear Panel Flutter with Piezoelectric Actuators Using Finite Element Method," *AIAA Journal*, Vol. 33, No. 6, 1995, pp. 1098–1105.

[10]Samanta, B., Ray, M. C., and Bhattacharyya, R., "Finite Element Model for Active Control of Intelligent Structures," *AIAA Journal*, Vol. 34, No. 9, 1996, pp. 1885–1893.

[11]Baz, A., and Poh, S., "Optimal Vibration Control with Modal Positive Position Feedback," *Optimal Control Applications and Methods*, Vol. 17, No. 2, 1996, pp. 141–149.

[12]Varadan, V. V., Kim, J., and Varadan, V. K., "Optimal Placement of Piezoelectric Actuators for Active Noise Control," *AIAA Journal*, Vol. 35, No. 3, 1997, pp. 526–533.

[13]Ray, M. C., "Optimal Control of Laminated Plates with Piezoelectric Sensor and Actuator Layers," *AIAA Journal*, Vol. 36, No. 12, 1998, pp. 2204–2208.

[14]Agarwal, B. N., and Treanor, K. E., "Shape Control of a Beam Using Piezoelectric Actuators," *Smart Materials and Structures*, Vol. 8, No. 6, 1999, pp. 729–740.

[15]Stöbener, U., and Gaul, L., "Modal Vibration Control for PVDF Coated Plates," *Journal of Intelligent Material Systems and Structures*, Vol. 11, No. 4, 2000, pp. 283–293.

[16]Sun, D. C., and Tong, L., "Vibration Control of Plates Using Discretely Distributed Piezoelectric Quasi-Modal Actuators/Sensors," *AIAA Journal*, Vol. 39, No. 9, 2001, pp. 1766–1772.

[17]Ray, M. C., "Optimal Control of Laminated Shells with Piezoelectric Sensor and Actuator Layers," *AIAA Journal*, Vol. 41, No. 6, 2003, pp. 1151–1157.

[18]Baz, A., and Ro, J., "Optimum Design and Control of Active Constrained Layer Damping," *Journal of Mechanical Design*, Vol. 117B, June 1995, pp. 135–144.

[19]Azvine, B., Tomlinson, G. R., and Wynne, R. J., "Use of Active Constrained Layer Damping for Controlling Resonant," *Smart Materials and Structures*, Vol. 4, No. 1, 1995, pp. 1–6.

[20]Baz, A., and Ro, J., "Vibration Control of Plates with Active Constrained Layer Damping," *Smart Materials and Structures*, Vol. 5, No. 3, 1996, pp. 272–280.

[21]Ray, M. C., and Baz, A., "Optimization of Energy Dissipation of Active Constrained Layer Damping Treatments of Plates," *Journal of Sound and Vibrations*, Vol. 208, No. 3, 1997, pp. 391–406.

[22]Ray, M. C., and Baz, A., "Control of Nonlinear Vibration of Beams Using Active Constrained Layer Damping Treatment," *Journal of Vibration and Control*, Vol. 7, No. 4, 2001, pp. 539–549.

[23]Ray, M. C., Oh, J., and Baz, A., "Active Constrained Layer Damping of Thin Cylindrical Shells," *Journal of Sound and Vibration*, Vol. 240, No. 5, 2001, pp. 921–935.

[24]Jeung, Y. S., and Shen, I. Y., "Development of Isoparametric, Degenerate Constrained Layer Element for Plate and Shell Structures," *AIAA Journal*, Vol. 39, No. 10, 2001, pp. 1997–2005.

[25]Chantalakhana, C., and Stanway, R., "Active Constrained Layer Damping of Clamped–Clamped Plate Vibrations," *Journal of Sound and Vibration*, Vol. 241, No. 5, 2001, pp. 755–777.

[26]Ro, J., and Baz, A., "Optimum Placement and Control of Active Constrained Layer Damping Using Modal Strain Energy Approach," *Journal of Vibration and Control*, Vol. 8, No. 6, 2002, pp. 861–876.

[27]Liu, Y., and Wang, K.-W., "Enhanced Active Constrained Layer Damping Treatment for Broadband Vibration Suppression," *Journal of Vibration and Control*, Vol. 8, No. 6, 2002, pp. 777–803.

[28]Gandhi, F., and Munskey, B. E., "Comparison of Damping Augmentation Mechanisms with Position and Velocity Feedback in Active Constrained Layer Treatments," *Journal of Intelligent Materials Systems and Structures*, Vol. 13, No. 5, 2002, pp. 326–335.

[29]Ray, M. C., and Reddy, J. N., "Optimal Control of Thin Circular Cylindrical Shells Using Active Constrained Layer Damping Treatment," *Smart Materials and Structures*, Vol. 13, No. 1, 2004, pp. 64–72.

[30]Smith, W. A., and Auld, B. A., "Modelling 1-3 Composite Piezoelectrics: Thickness Mode Oscillations," *IEEE Transactions on Ultrasonics, Ferroelectrics, and Frequency Control*, Vol. 38, No. 1, 1991, pp. 40–47.

[31]Aboudi, J., "Micromechanical Prediction of the Effective Coefficients of Thermopiezoelectric Multiphase Composites," *Journal of Intelligent Material Systems and Structures*, Vol. 9, No. 9, 1998, pp. 713–722.

[32]Sigmud, O., Torquato, S., and Aksay, I. A., "On the Design of 1-3 Piezocomposite Using Topology Optimization," *Journal of Material Research*, Vol. 13, No. 4, 1998, pp. 1038–1048.

[33]Mallik, N., and Ray, M. C., "Effective Coefficients of Piezoelectric Fiber Reinforced Composites," *AIAA Journal*, Vol. 41, No. 4, 2003, pp. 704–710.

[34]Ray, M. C., and Mallik, N., "Active Control of Laminated Composite Beams Using a Piezoelectric Fiber Reinforced Composite Layer," *Smart Materials and Structures*, Vol. 13, No. 1, 2004, pp. 146–152.

[35]Ray, M. C., and Mallik, N., "Finite Element Solutions for Static Analysis of Smart Structures with a Layer of Piezoelectric Fiber Reinforced Composites," *AIAA Journal*, Vol. 42, No. 7, 2004, pp. 1398–1405.

[36]Reddy, J. N., *Mechanics of Laminated Composite Plates Theory and Analysis*, CRC Press, Boca Raton, FL, 1996.

[37]Tiersten, H. F., *Linear Piezoelectric Plate Vibration*, Plenum, New York, 1969.

[38]Ray, M. C., "Zeroth Order Shear Deformation Theory for Laminated Composite Plates," *Journal of Applied Mechanics*, Vol. 70, May 2003, pp. 374–380.

M. Ahmadian
Associate Editor